Hindawi Publishing Corporation
Computational and Mathematical Methods in Medicine
Volume 2016, Article ID 6189374, 12 pages
http://dx.doi.org/10.1155/2016/6189374

Research Article

Effects of Na^+ Current and Mechanogated Channels in Myofibroblasts on Myocyte Excitability and Repolarization

Heqing Zhan,[1] Jingtao Zhang,[2] Jialun Lin,[1] and Guilai Han[1]

[1]*Department of Information Technology, Hainan Medical University, Haikou 571199, China*
[2]*Cardiac Arrhythmia Center, Fuwai Hospital, National Center for Cardiovascular Diseases, Beijing 100037, China*

Correspondence should be addressed to Heqing Zhan; zhq86zijing@163.com

Received 4 July 2016; Revised 9 October 2016; Accepted 19 October 2016

Academic Editor: Marko Gosak

Fibrotic remodeling, characterized by fibroblast phenotype switching, is often associated with atrial fibrillation and heart failure. This study aimed to investigate the effects on electrotonic myofibroblast-myocyte (Mfb-M) coupling on cardiac myocytes excitability and repolarization of the voltage-gated sodium channels (VGSCs) and single mechanogated channels (MGCs) in human atrial Mfbs. Mathematical modeling was developed from a combination of (1) models of the human atrial myocyte (including the stretch activated ion channel current, I_{SAC}) and Mfb and (2) our formulation of currents through VGSCs (I_{Na_Mfb}) and MGCs (I_{MGC_Mfb}) based upon experimental findings. The effects of changes in the intercellular coupling conductance, the number of coupled Mfbs, and the basic cycle length on the myocyte action potential were simulated. The results demonstrated that the integration of I_{SAC}, I_{Na_Mfb}, and I_{MGC_Mfb} reduced the amplitude of the myocyte membrane potential (V_{max}) and the action potential duration (APD), increased the depolarization of the resting myocyte membrane potential (V_{rest}), and made it easy to trigger spontaneous excitement in myocytes. For Mfbs, significant electrotonic depolarizations were exhibited with the addition of I_{Na_Mfb} and I_{MGC_Mfb}. Our results indicated that I_{SAC}, I_{Na_Mfb}, and I_{MGC_Mfb} significantly influenced myocytes and Mfbs properties and should be considered in future cardiac pathological mathematical modeling.

1. Introduction

Recent studies have demonstrated a correlation between atrial fibrillation (AF) and fibrotic remodeling, specifically fibrosis [1–3]. However, their relationship has not been fully understood. Changes have taken place during the process of fibrotic remodeling in terms of gap junction remodeling [4], the deposition of excess collagen [5], and fibroblast phenotype switching [2, 6], which determines the degree of AF initiation and maintenance in atrial fibrosis in AF subjects [7].

Different currents have been identified in cardiac fibroblasts by recent electrophysiological studies, including the currents through potassium channels [8, 9], the nonselective transient receptor potential cationic channel subfamily M member 7 (TRPM7) [10], voltage-gated sodium channels (VGSCs) [11], chloride channels [12], single mechanogated channels (MGCs) [13], and voltage-dependent proton currents [14]. Therefore, fibroblasts are no longer considered as nonexcitable cells. As one of the main characteristics of fibrotic remodeling, fibroblasts proliferation and differentiation into myofibroblasts (Mfbs) at the cellular level have been shown to play an important role in cardiac pathological status [15, 16]. During fibroblasts differentiation, significantly increased potassium channels and TRPM7 have been reported [10, 17]. Specifically, with the measurement of the neoexpression of rapid Na^+ currents through VGSCs during the process, 75% of the Mfbs derived from the culture of human atrial fibroblasts expressed Na^+ current between 8 and 12 days. After 12 days, 100% of the Mfbs expressed Na^+ current [11]. In addition, there is strong evidence that this Na^+ current is generated by Na_v 1.5 α-subunit, a typical VGSC to produce Na^+ current in cardiomyocytes [11].

Recent studies have also suggested that MGCs were modulated by mechanical deformations of fibroblasts, which may contribute to the cardiac mechanoelectrical feedback under both physiological and pathophysiological conditions [18, 19]. As myocytes start contracting, the interposed fibroblasts

are mechanically compressed. The membrane potential of fibroblasts is depolarized by ionic currents through MGCs [13, 18].

Computational models of atrial fibrosis have been used to investigate the relationship between fibrotic remodeling and AF. For gap junction remodeling, simulation results showed that increased anisotropy led to sustained reentrant activity [20]. For collagen deposition, it has been demonstrated that patchy distributions of collagen were responsible for atrial conduction disturbances in failing hearts [21, 22]. For fibroblast proliferation and phenotype switching, studies indicated that coupling of fibroblasts to atrial myocytes resulted in shorter duration of the action potential (APD), slower conduction, and the development of AF [23, 24]. Taking Mfbs into account, other studies combined all the above-mentioned elements in the left atrial model to examine the underlying mechanisms of AF initiation and indicated that Mfbs exerted electrotonic influences on myocytes in the lesions [1, 25]. However, all these published simulation studies have not considered the following: first, the stretch activated ion channel current (I_{SAC}) in myocytes, which significantly influences the electrophysiological characteristics of cardiac myocytes under stretching [26, 27]; second, the currents through VGSCs (I_{Na_Mfb}) and MGCs (I_{MGC_Mfb}) in Mfbs, which could influence Mfb properties and contribute to mechanoelectrical coupling in cardiac pathologies [11, 13].

The present study aimed to investigate the combinational role of I_{SAC}, I_{Na_Mfb}, and I_{MGC_Mfb} in the excitability and repolarization of cardiac myocytes by Mfb-myocyte (Mfb-M) coupling. Specifically, a new formulation of I_{Na_Mfb} and I_{MGC_Mfb} based on experimental data will be combined with models of human atrial myocyte (including I_{SAC}) and Mfb. Simulation results of human atrial myocyte action potential (AP) dynamics from different gap-junctional conductances (G_{gap}), number of coupled Mfbs, and basic cycle lengths (BCLs) will be compared.

2. Materials and Methods

The framework of the coupled Mfb-M model was developed from Maleckar et al.'s model of the human atrial myocyte [28] (including I_{SAC} equations described by Kuijpers et al. [26]), MacCannell et al.'s model of the human cardiac Mfb [24], and our new formulation of I_{Na_Mfb} and I_{MGC_Mfb} based on experimental findings from Chatelier et al. [11] and Kamkin et al. [13]. Figure 1 is a schematic of the Mfb-M coupling model. An overview of the simulations is described as follows.

2.1. Mfb-M Coupling. According to [24], the differential equations for the membrane potential of cardiac Mfb and myocyte are given by

$$\frac{dV_{\mathrm{Mfb},i}}{dt} = -\frac{1}{C_{m,\mathrm{Mfb}}}\left(I_{\mathrm{Mfb},i}\left(V_{\mathrm{Mfb},i}, t\right) + G_{\mathrm{gap}}\left(V_{\mathrm{Mfb},i} - V_M\right)\right), \quad (1)$$

$$\frac{dV_M}{dt} = -\frac{1}{C_{m,M}}\left(I_M\left(V_M, t\right) + \sum_{i=1}^{n} G_{\mathrm{gap}}\left(V_M - V_{\mathrm{Mfb},i}\right)\right),$$

where $V_{\mathrm{Mfb},i}$ and V_M represent the transmembrane potential of the ith coupled Mfb and the human atrial myocyte, respectively; $C_{m,\mathrm{Mfb}}$ and $C_{m,M}$ represent the membrane capacitance of the Mfb and the myocyte, respectively; $I_{\mathrm{Mfb},i}$ and I_M represent the transmembrane current of the ith coupled Mfb and the human atrial myocyte, respectively; and G_{gap} represents the gap-junctional conductance, which varies between 0.5 and 8 nS in individual simulations based on previous measurements [19, 29]. A negative I_{gap} (i.e., $G_{\mathrm{gap}}\left(V_{\mathrm{Mfb},i} - V_M\right)$) indicates that the current is flowing from the myocyte into the ith Mfb, and n is the total number of coupled Mfbs.

2.2. Mathematical Model of the Human Atrial Myocyte. The mathematical model from Maleckar et al. was implemented in this study [28], which was based on experimental data and has correctly replicated APD restitution of the adult human atrial myocyte. To describe the influence of stretch on myocyte AP, the original model from Maleckar et al. was modified with the total ionic current of myocyte (I_M) given by

$$\begin{aligned} I_M\left(V_M, t\right) = {} & I_{\mathrm{Na}} + I_{\mathrm{CaL}} + I_{\mathrm{t}} + I_{\mathrm{Kur}} + I_{\mathrm{Kl}} + I_{\mathrm{K,r}} + I_{\mathrm{K,s}} \\ & + I_{\mathrm{B,Na}} + I_{\mathrm{B,Ca}} + I_{\mathrm{NaK}} + I_{\mathrm{CaP}} + I_{\mathrm{NaCa}} \\ & + I_{\mathrm{SAC}} - I_{\mathrm{Stim}}, \end{aligned} \quad (2)$$

where I_{Na} is fast inward Na^+ current; I_{CaL} is L-type Ca^{2+} current; I_{t} is transient outward K^+ current; I_{Kur} is sustained outward K^+ current; I_{Kl} is inward rectifying K^+ current; $I_{\mathrm{K,r}}$ is rapid delayed rectifier K^+ current; $I_{\mathrm{K,s}}$ is slow delayed rectifier K^+ current; $I_{\mathrm{B,Na}}$ is background Na^+ current; $I_{\mathrm{B,Ca}}$ is background Ca^{2+} current; I_{NaK} is Na^+-K^+ pump current; I_{CaP} is sarcolemmal Ca^{2+} pump current; I_{NaCa} is Na^+-Ca^{2+} exchange current; I_{SAC} is stretch activated current; and I_{Stim} is stimulated current.

On the basis of experimental observations [30], it has been reported by Kuijpers et al. that I_{SAC} in atrial myocytes is permeable to Na^+, K^+, and Ca^{2+} [26], which is defined as

$$I_{\mathrm{SAC}} = I_{\mathrm{SAC,Na}} + I_{\mathrm{SAC,K}} + I_{\mathrm{SAC,Ca}}, \quad (3)$$

where $I_{\mathrm{SAC,Na}}$, $I_{\mathrm{SAC,K}}$, and $I_{\mathrm{SAC,Ca}}$ represent the contributions of Na^+, K^+, and Ca^{2+} to I_{SAC}, respectively. These currents were defined by the constant-field Goldman-Hodgkin-Katz current equation [26].

To introduce the effect of I_{SAC} on intracellular Na^+, K^+, and Ca^{2+} concentrations ($[Na^+]_i$, $[K^+]_i$, and $[Ca^{2+}]_i$), we replaced equations of $[Na^+]_i$, $[K^+]_i$, and $[Ca^{2+}]_i$ in Maleckar et al.'s model [28] by

$$\frac{d\left[\mathrm{Na}^+\right]_i}{dt} = -\frac{I_{\mathrm{Na}} + I_{\mathrm{B,Na}} + 3I_{\mathrm{NaK}} + 3I_{\mathrm{NaCa}} + I_{\mathrm{SAC,Na}}}{\mathrm{Vol}_i F},$$

$$\frac{d\left[\mathrm{K}^+\right]_i}{dt} = -\frac{I_{\mathrm{t}} + I_{\mathrm{Kur}} + I_{\mathrm{Kl}} + I_{\mathrm{K,s}} + I_{\mathrm{K,r}} - 2I_{\mathrm{NaK}} + I_{\mathrm{SAC,K}}}{\mathrm{Vol}_i F},$$

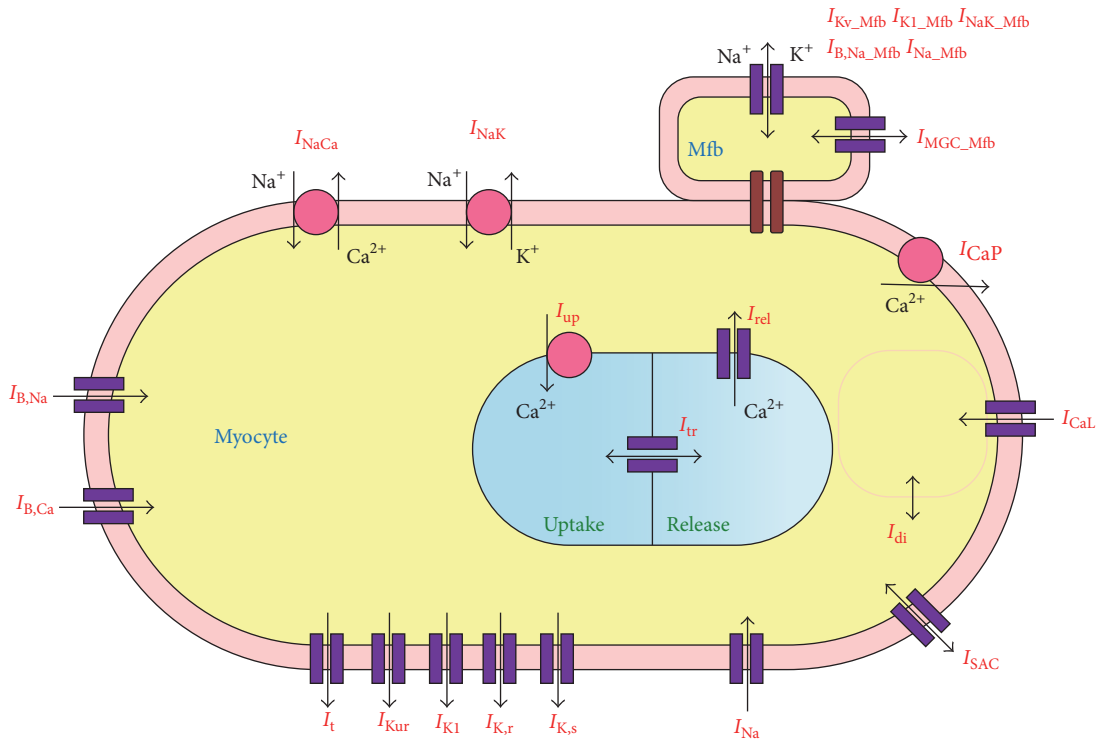

FIGURE 1: Schematic representation of the mathematical model of Mfb-M coupling.

$$\frac{d\left[Ca^{2+}\right]_i}{dt} = -\frac{-I_{di} + I_{B,Ca} + I_{CaP} - 2I_{NaCa} + I_{up} - I_{rel} + I_{SAC,Ca}}{2.0 Vol_i F} - \frac{dO}{dt}, \quad (4)$$

where F is Faraday's constant; Vol_i is cytosolic volume; I_{di} is Ca^{2+} diffusion current from the diffusion-restricted subsarcolemmal space to the cytosol; I_{up} is sarcoplasmic reticulum Ca^{2+} uptake current; I_{rel} is sarcoplasmic reticulum Ca^{2+} release current; and O is buffer occupancy.

2.3. Electrophysiological Model of the Human Atrial Mfb. The electrophysiological model of the human atrial Mfb from MacCannell et al. [24] was used in the present study. It included time- and voltage-dependent K^+ current (I_{Kv_Mfb}), inward rectifying K^+ current (I_{K1_Mfb}), Na^+-K^+ pump current (I_{NaK_Mfb}), and Na^+ background current (I_{B,Na_Mfb}).

In addition, I_{Na_Mfb} and I_{MGC_Mfb} were added in the Mfb model. According to the published experimental data [9], the Mfb transmembrane potential V_{Mfb} and $C_{m,Mfb}$ of −47.75 mV and 6.3 pF were used.

For I_{Na_Mfb}, the steady-state value of activation gating variable for Na^+ current ($\overline{m}_{Mfb}$) was obtained by fitting the experimental data from Chatelier et al. [11] with a Boltzmann function using Origin software:

$$y = \frac{A_1 - A_2}{1 + e^{(V_{Mfb} - V_{0.5})/k}} + A_2, \quad (5)$$

where V_{Mfb} is the Mfb potential ranging from −120 mV to 40 mV in 10 mV increments and y is the corresponding value of $\overline{m}_{Mfb}$ at each V_{Mfb}. A_1 and A_2 are fitting coefficients and $V_{0.5}$ and k represent the half-maximum voltage of activation and the Boltzmann steepness coefficient, respectively.

After the data were fitted with a Boltzmann function, A_1 and A_2 were −0.0102 and 1.0063, respectively. $V_{0.5}$ and k were −42.1 mV and 10.53, respectively. The equation of $\overline{m}_{Mfb}$ was then expressed as

$$\overline{m}_{Mfb} = \frac{-0.0102 - 1.0063}{1.0 + e^{(V_{Mfb} + 42.1)/10.53}} + 1.0063. \quad (6)$$

The steady-state value of inactivation gating variable for I_{Na_Mfb} ($\overline{j}_{Mfb}$) was also fitted with the Boltzmann function, with A_1 and A_2 of 1.04 and 0.004 and $V_{0.5}$ and k of −84.82 mV and 9.4, respectively. The equation of $\overline{j}_{Mfb}$ was given as

$$\overline{j}_{Mfb} = \frac{1.04 - 0.004}{1.0 + e^{(V_{Mfb} + 84.82)/9.4}} + 0.004. \quad (7)$$

As suggested by Chatelier et al. that I_{Na_Mfb} was generated by the same Na_v 1.5 which produced Na^+ currents in the atria and ventricle of the adult human heart [11], the equations of activation time constants in the model of Courtemanche et

al. [31] were used to describe the activation time constant for $I_{\text{Na\_Mfb}}$ ($\tau_{m_{\text{Mfb}}}$). The equations are given by

$$\alpha_{m_{\text{Mfb}}} = A_1 \frac{V_{\text{Mfb}} + V_x}{1 - e^{A_2(V_{\text{Mfb}}+V_x)}}, \tag{8}$$

$$\beta_{m_{\text{Mfb}}} = A_3 e^{-V_{\text{Mfb}}/A_4}, \tag{9}$$

$$\tau_{m_{\text{Mfb}}} = \frac{1}{\alpha_{m_{\text{Mfb}}} + \beta_{m_{\text{Mfb}}}}, \tag{10}$$

where V_{Mfb} are original values, ranging from −40 mV to 30 mV in 10 mV increments and $\tau_{m_{\text{Mfb}}}$ is the corresponding value at each V_{Mfb}. $\alpha_{m_{\text{Mfb}}}$ and $\beta_{m_{\text{Mfb}}}$ are extrapolated rate coefficients. After the data were fitted with these equations, A_1 to A_4 were 0.0077, −0.18, 0.004, and 11.98, and V_x was 68.19 mV.

Equation (8) requires evaluation of a limit to determine the value at membrane potential for which its denominator is zero. Equations (8) and (9) are therefore expressed as follows:

$$\alpha_{m_{\text{Mfb}}} = \begin{cases} 0.0077 \dfrac{V_{\text{Mfb}} + 68.19}{1.0 - e^{-0.18(V_{\text{Mfb}}+68.19)}} & \\ 0.0433, & \text{if } V_{\text{Mfb}} = -68.19 \end{cases} \tag{11}$$

$$\beta_{m_{\text{Mfb}}} = 0.004 e^{-V_{\text{Mfb}}/11.98}.$$

Similarly, the equations of inactivation time constant ($\tau_{j_{\text{Mfb}}}$) were as follows:

$$\begin{aligned} \alpha_{j_{\text{Mfb}}} &= \begin{cases} \left(-14.5 e^{0.17 V_{\text{Mfb}}} + 1.8 e^{1.56 V_{\text{Mfb}}}\right) \cdot \dfrac{V_{\text{Mfb}} + 35.73}{1.0 + e^{3.31(V_{\text{Mfb}}+3.86)}} & \\ 0, & \text{if } V_{\text{Mfb}} \geq -40.0, \end{cases} \\ \beta_{j_{\text{Mfb}}} &= \begin{cases} 5.05 \times 10^{-5} \dfrac{e^{-0.0995 V_{\text{Mfb}}}}{1.0 + e^{-0.01(V_{\text{Mfb}}-84.02)}} & \\ 0.11 \dfrac{e^{-4.13\times10^{-4} V_{\text{Mfb}}}}{1.0 + e^{-0.09(V_{\text{Mfb}}+42.44)}}, & \text{if } V_{\text{Mfb}} \geq -40.0, \end{cases} \\ \tau_{j_{\text{Mfb}}} &= \frac{1}{\alpha_{j_{\text{Mfb}}} + \beta_{j_{\text{Mfb}}}}. \end{aligned} \tag{12}$$

The model of $I_{\text{Na\_Mfb}}$ was modified from the equation described by Luo and Rudy [32], as follows:

$$\begin{aligned} I_{\text{Na\_Mfb}} &= \overline{g}_{\text{Na,Mfb}} m_{\text{Mfb}} j_{\text{Mfb}}^{0.12} \left(V_{\text{Mfb}} - E_{\text{Na,Mfb}}\right), \\ E_{\text{Na,Mfb}} &= \frac{\text{RT}}{F} \log \frac{\left[\text{Na}^+\right]_{c,\text{Mfb}}}{\left[\text{Na}^+\right]_{i,\text{Mfb}}}, \end{aligned} \tag{13}$$

where $\overline{g}_{\text{Na,Mfb}}$, the maximum conductance of $I_{\text{Na\_Mfb}}$, was 0.756 nS; $E_{\text{Na,Mfb}}$ is the Nernst potential for Na^+ ions; $[Na^+]_{c,\text{Mfb}}$, the Mfb extracellular Na^+ concentration, was 130.011 mmol/L; $[Na^+]_{i,\text{Mfb}}$, the Mfb intracellular Na^+ concentration, initial value was 8.5547 mmol/L; m_{Mfb} and j_{Mfb} were the activation and inactivation parameters, respectively. In order to conform to the experiment data [11], j was modified to be $j^{0.12}$. Equations of time dependence were given by

$$\begin{aligned} \frac{dm_{\text{Mfb}}}{dt} &= \frac{\overline{m}_{\text{Mfb}} - m_{\text{Mfb}}}{\tau_{m_{\text{Mfb}}}}, \\ \frac{dj_{\text{Mfb}}}{dt} &= \frac{\overline{j}_{\text{Mfb}} - j_{\text{Mfb}}}{\tau_{j_{\text{Mfb}}}}. \end{aligned} \tag{14}$$

For $I_{\text{MGC\_Mfb}}$, the equation based on experimental results from Kamkin et al. [13] was given by

$$I_{\text{MGC\_Mfb}} = \overline{g}_{\text{MGC,Mfb}} \cdot \left(V_{\text{Mfb}} - E_{\text{MGC,Mfb}}\right), \tag{15}$$

where $\overline{g}_{\text{MGC,Mfb}}$, the maximum conductance of $I_{\text{MGC\_Mfb}}$, was 0.043 nS and $E_{\text{MGC,Mfb}}$, the reversal potential of MGCs, was close to 0 mV [13].

2.4. Simulation Protocol. Simulations were carried out with (1) two Mfbs coupled to a single atrial myocyte in which G_{gap} varied between 0.5 and 8 nS and (2) one and four identical Mfbs coupled to a single atrial myocyte at constant G_{gap} of 3 nS. Next, in order to investigate the role of BCL in myocyte AP, the coupled system was paced with BCLs from 100 to 2000 ms for each G_{gap} (0.5 or 8 nS) and for each number of coupled Mfbs (1 or 4). The resting myocyte membrane potential (V_{rest}), the amplitude of the myocyte membrane potential (V_{max}), and APD at 90% repolarization (APD_{90}) at different BCLs were obtained.

To ensure that the coupled system reached steady state, stimulation was repeated for 20 cycles. The results from the last cycle in each simulation were used. All state variables of the coupled model were updated by means of the forward Euler method. The time step was set to be 10 μs to ensure numerical accuracy and stability.

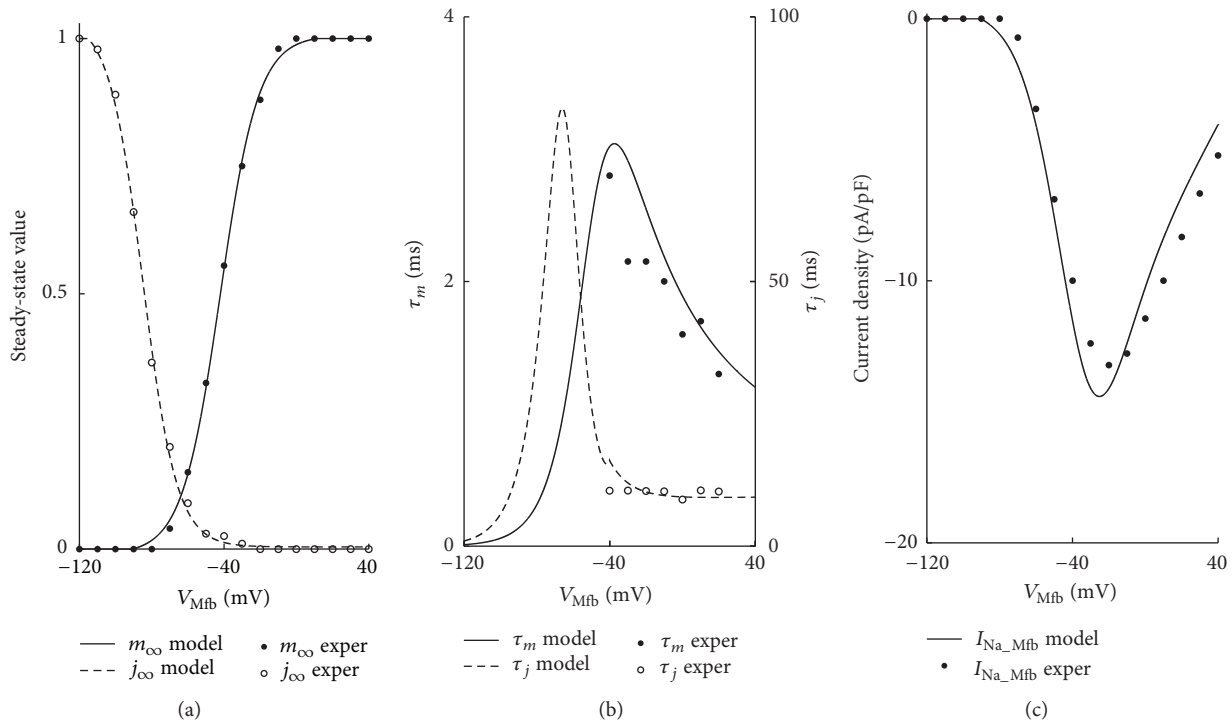

FIGURE 2: Model representation of parameters describing I_{Na_Mfb}. (a) Steady-state activation (solid line) and inactivation (dashed line) curves, (b) gating variable fast (solid line) and slow (dashed line) time constants, and (c) I-V relationship (solid line). Experimental data (filled and hollow circles) from Chatelier et al. is included for comparison.

3. Results

3.1. I_{Na_Mfb} and I_{MGC_Mfb} in Mfbs. Figure 2 shows the steady-state activation and inactivation curves, time constants, and the current-voltage (I-V) relationship of I_{Na_Mfb}. All the curves were consistent with the experimental data [11].

Figure 3 shows the linear I-V relationship of I_{MGC_Mfb}. The curve was consistent with the experimental data [13].

3.2. Effects of I_{SAC}, I_{Na_Mfb}, and I_{MGC_Mfb} on Atrial Myocyte and Mfbs. Figure 4 shows the combinational effects of I_{SAC}, I_{Na_Mfb}, and I_{MGC_Mfb} on the membrane potential of myocytes and Mfbs by coupling two Mfbs to a human atrial myocyte with G_{gap} of 0.5 and 8 nS. For myocytes, including I_{Na_Mfb}, I_{SAC} and I_{MGC_Mfb} to the model of Mfb-M coupling resulted in gradually decreased V_{max} and APD_{90} and increased V_{rest} depolarization (Figures 4(a) and 4(b)). With G_{gap} of 0.5 nS, V_{max} was decreased by 0.8% (with I_{Na_Mfb}), 16.7% (with I_{Na_Mfb} and I_{SAC}), and 18.6% (with I_{Na_Mfb}, I_{SAC}, and I_{MGC_Mfb}) in comparison with the control (without I_{Na_Mfb}, I_{SAC}, and I_{MGC_Mfb}). Correspondingly, for the three conditions, APD_{90} was decreased by 20.0%, 19.1%, and 20.2%, respectively, and V_{rest} increased by 8.3%, 20.3%, and 22.4%, respectively. With G_{gap} of 8 nS, V_{max} was decreased by 0.2%, 23.5%, and 18.6%, respectively. APD_{90} was decreased by 1.6%, 4.1%, and 11.1%, respectively. V_{rest} was increased by 0.8%, 12.5%, and 15.9%, respectively. In addition, I_{Na_Mfb}, I_{SAC}, and I_{MGC_Mfb} decelerated the repolarization of the atrial myocyte AP, especially with a large G_{gap}. For Mfbs, with G_{gap} of 0.5 nS, significant

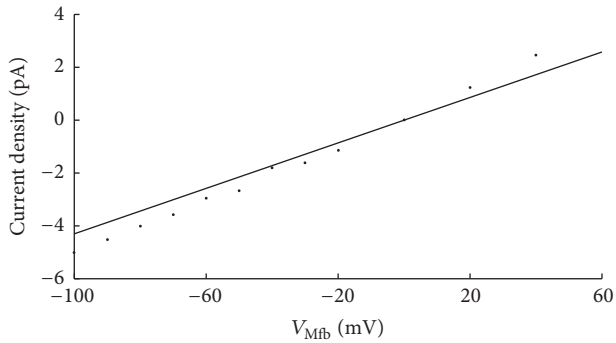

FIGURE 3: The I-V relationship (solid line) of MGCs. Experimental data (filled circles) from Kamkin et al. is included for comparison.

electrotonic depolarizations were observed with the integration of the three currents (Figure 4(c)). V_{max} of the Mfb was −12.4 mV (control), 7.1 mV (with I_{Na_Mfb}), 1.5 mV (with I_{Na_Mfb} and I_{SAC}), and −1.0 mV (with I_{Na_Mfb}, I_{SAC}, and I_{MGC_Mfb}), respectively. With G_{gap} of 8 ns, the effects of these currents on Mfbs were similar with that on myocytes (Figure 4(d)).

Figure 5 illustrates similar effects of I_{SAC}, I_{Na_Mfb}, and I_{MGC_Mfb} on the membrane potential of myocytes and Mfbs when G_{gap} was fixed at 3 nS and the number of coupled Mfbs was one or four. For myocytes, integrating these currents into the coupled model resulted in decreased V_{max} and APD_{90} and greater depolarization in V_{rest} (Figures 5(a) and 5(b)). Coupling one Mfb to a human atrial myocyte resulted in

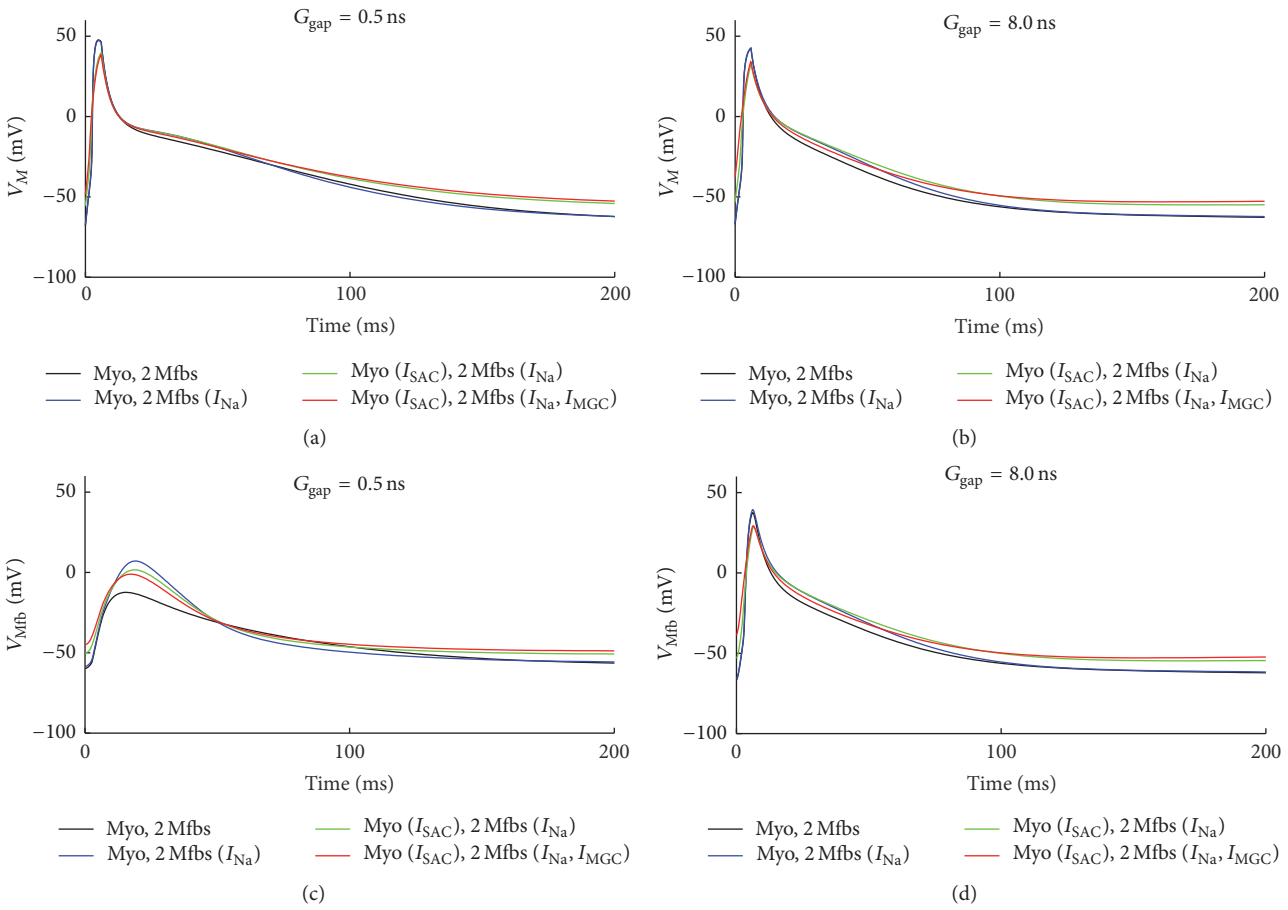

FIGURE 4: Effects of I_{SAC}, I_{Na_Mfb}, and I_{MGC_Mfb} on transmembrane potential of myocyte and Mfb. (a, b) V_M and (c, d) V_{Mfb}, in Mfb-M coupling with I_{Na_Mfb} (blue line), with I_{SAC} and I_{Na_Mfb} (green line), and with I_{SAC}, I_{Na_Mfb}, and I_{MGC} (red line) as compared to control (black line), by coupling two Mfbs to an atrial myocyte with G_{gap} of 0.5 and 8 nS.

0.1% (with I_{Na_Mfb}), 38.1% (with I_{Na_Mfb} and I_{SAC}), and 37.4% (with I_{Na_Mfb}, I_{SAC}, and I_{MGC_Mfb}) decreases in V_{max} when compared with the control. Correspondingly, APD_{90} was decreased by 1.1%, 7.7%, and 7.8%, and V_{rest} increased by 0.4%, 25.0%, and 28.6%, respectively. Similarly, coupling four Mfbs to a human atrial myocyte resulted in 7.9%, 30.3%, and 25.9% decreases in V_{max} when compared with the control. APD_{90} was decreased by 1.6%, 8.9%, and 18.9%, and V_{rest} was increased by 2.3%, 17.4%, and 23.6%, respectively. For Mfbs, the effects of these currents were similar with that on myocytes (Figures 5(c) and 5(d)).

Figure 6 illustrates the changes of V_{rest}, V_{max}, and APD_{90} in myocyte with the integration of I_{SAC}, I_{Na_Mfb}, and I_{MGC_Mfb} as a function of BCL when coupling two Mfbs to a human atrial myocyte. For both low (0.5 nS, Figures 6(a), 6(c), and 6(e)) and high (8 nS, Figures 6(b), 6(d), and 6(f)) G_{gap}, V_{rest} declined and V_{max} rose in the control and with I_{Na_Mfb} as BCL increased (Figures 6(a) to 6(d)). V_{rest} decreased initially and then increased slightly with I_{SAC} and I_{Na_Mfb} and with I_{SAC}, I_{Na_Mfb}, and I_{MGC_Mfb}. Contrarily, V_{max} increased with BCL initially and then decreased slightly. Gaps of V_{rest} and V_{max} between the four cases widened as the BCL increased with more pronounced variations for the high G_{gap}. APD_{90} was prolonged as BCL increased in all the four situations for both G_{gap} values (Figures 6(e) and 6(f)). With G_{gap} of 0.5 nS, similar to V_{max}, APD_{90} gradually dropped with I_{Na_Mfb}, I_{SAC}, and I_{MGC_Mfb} in order at each BCL. However, there was no obvious difference between the four situations with G_{gap} of 8 nS.

Figure 7 shows the APs of the human atrial myocyte at the 20st cycle with BCL of 100 (Figures 7(a) and 7(b)), 500 (Figures 7(c) and 7(d)), 1000 (Figures 7(e) and 7(f)), and 2000 ms (Figures 7(g) and 7(h)) when G_{gap} was fixed at 3 nS and the number of coupled Mfbs was one or four. Integrating I_{SAC}, I_{Na_Mfb}, and I_{MGC_Mfb} into the model of Mfb-M coupling resulted in reductions in V_{max} and APD_{90} and greater depolarization in V_{rest}. However, it is noted that spontaneous excitements in the myocyte appeared when the value of BCL was higher than a certain value (1000 ms in this study). The increased V_{rest} and the longer stimulus interval were the two major factors for the spontaneous excitement. Meanwhile, integrating I_{SAC}, I_{Na_Mfb}, and I_{MGC_Mfb} simultaneously into the coupled model triggered the most and earliest spontaneous excitement at BCL of 1000 and 2000 ms, suggesting that the three currents could result in discordant alternans, especially with large BCL (2000 ms in this study).

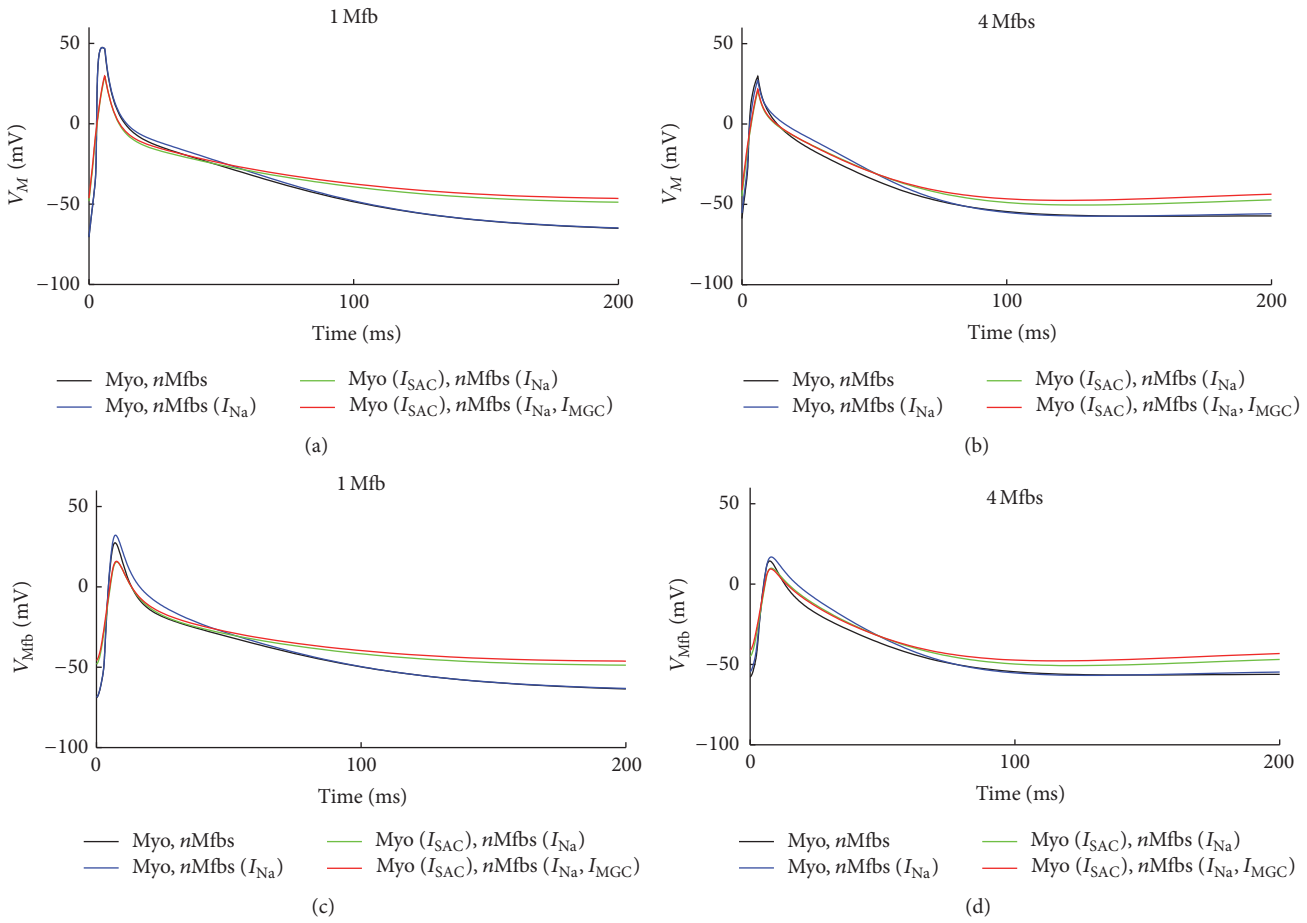

FIGURE 5: Effects of I_{SAC}, I_{Na_Mfb}, and I_{MGC_Mfb} on transmembrane potential of myocyte and Mfb. (a, b) V_M and (c, d) V_{Mfb}, in Mfb-M coupling with I_{Na_Mfb} (blue line), with I_{SAC} and I_{Na_Mfb} (green line), and with I_{SAC}, I_{Na_Mfb} and I_{MGC} (red line) as compared to control (black line), by coupling one and four Mfbs to an atrial myocyte with G_{gap} of 3 nS.

4. Discussion

This study investigated the roles of I_{SAC}, I_{Na_Mfb}, and I_{MGC_Mfb} in the excitability and AP. To address these issues, numerical simulations of the coupled Mfb-M system were performed by employing a combination of models of the human atrial myocyte (including I_{SAC}) and Mfb, as well as modified formulation of I_{Na_Mfb} and I_{MGC_Mfb} based on experimental data. Specifically, the effects of these currents with changes in (1) G_{gap}, (2) the number of Mfbs, and (3) BCL on the human atrial myocyte AP dynamics were investigated. The main results with the integration of I_{SAC}, I_{Na_Mfb}, and I_{MGC_Mfb} were as follows: (1) for myocytes, the addition of I_{SAC}, I_{Na_Mfb}, and I_{MGC_Mfb} resulted in decreased V_{max} and APD_{90} and increased V_{rest} depolarization; deceleration of AP repolarization; and trigger of spontaneous excitements even discordant alternans at large BCLs and (2) for Mfbs, significant electrotonic depolarizations were obtained with small G_{gap}. As the value of G_{gap} and the number of coupled Mfbs increased, the effects for Mfbs were similar to those in myocytes.

4.1. Resting Potential of Human Atrial Mfbs. V_{rest} of fibroblasts/Mfbs in human atria was close to −15 mV [33, 34]. At this potential, the persistent entry of Na^+ in Mfb would be negligible [11]. Indeed, it has been reported that V_{rest} of these cells was sensitive to mechanical stress under both contraction and relaxation [13, 35, 36]. A stretch of 3 μm led to a negative shift of V_{rest}, about −35 ± 5 mV [13]. Reoxygenation after hypoxia also produced a hyperpolarization to V_{rest} [37]. Based on these findings, we set up the mathematical formulation of I_{MGC_Mfb} and included it in the Mfb-M coupling model. In addition, it has also been shown that K^+ current in cardiac fibroblasts and V_{rest} was between −40.0 and −60.0 mV [8, 9, 38]. These potentials corresponded to the peak of the Na^+ window current described by Chatelier et al. [11]. A persistent Na^+ entry may be induced based on such a cell polarity. Therefore, we also introduced the mathematical formulation of I_{Na_Mfb} and included it in Mfb modeling. V_{rest} was set to be −47.8 mV, within the range of experimental findings [8, 9].

4.2. Role of I_{SAC}, I_{Na_Mfb}, and I_{MGC_Mfb} on V_{rest} and Excitability of Human Atrial Myocytes. Both experimental data and computational work have shown that the value of G_{gap} and the number of coupled fibroblasts/Mfbs were important in determining the depolarization of the coupled human myocyte at rest [24, 28, 29, 39]. Based on the preceding

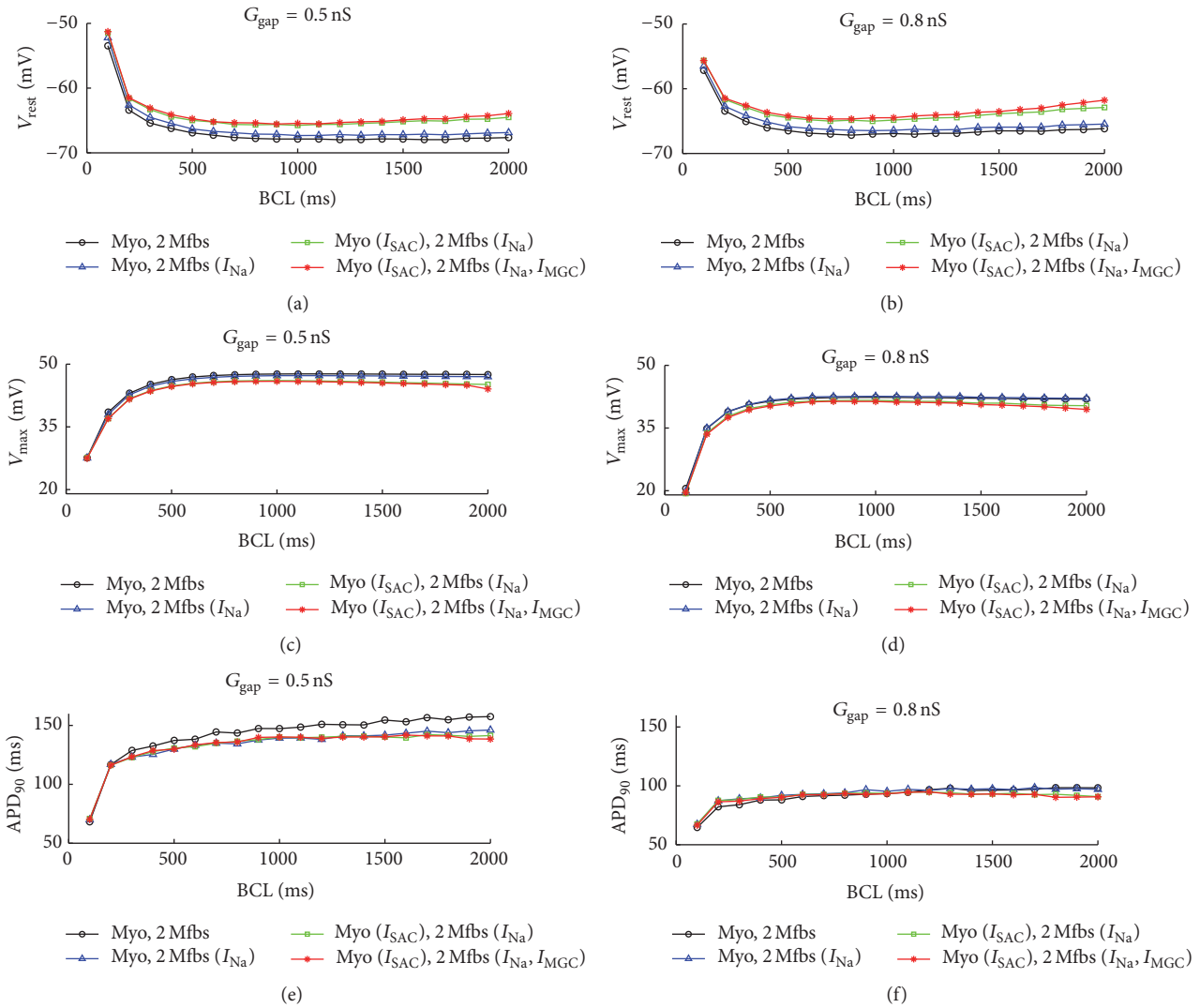

FIGURE 6: Effects of I_{SAC}, I_{Na_Mfb}, and I_{MGC_Mfb} on AP characteristics as a function of BCL in Mfb-M coupling with I_{Na_Mfb} (blue line with hollow triangle), with I_{SAC} and I_{Na_Mfb} (green line with hollow rectangle), and with I_{SAC}, I_{Na_Mfb}, and I_{MGC} (red line with asterisk) as compared to control (black line with hollow circle), by coupling two Mfbs to an atrial myocyte with G_{gap} of 0.5 and 8 nS. (a, b) V_{rest}, (c, d) V_{max}, and (e, f) APD_{90}.

conclusions, our simulations also considered the effects of I_{SAC}, I_{Na_Mfb}, and I_{MGC_Mfb} on V_{rest} and excitability of human atrial myocytes.

For I_{SAC}, previous studies explored the electrophysiological effect of sustained stretch and indicated that I_{SAC} influenced cardiac myocytes repolarization and activation [26, 40]. With pathophysiological conditions, such as hypertension and AF, it has been observed that atrial stretch and dilatation influenced atrial flutter cycle length and facilitated the induction and maintenance of AF [41, 42]. However, the SAC blocker Gd^{3+} reduced the stretch-induced vulnerability to AF [43]. These observational studies confirmed that I_{SAC} plays a significant role in heart pathology. In our simulations, integrating I_{SAC} into the mathematical model of the human atrial myocyte resulted in a significant depolarization of V_{rest} and prolongation of repolarization (Figures 4 to 7). These phenomena led to alternating spontaneous excitement propagation at a BCL of 2000 ms (Figure 7). Our simulation agreed with Kuijpers et al., where slow conduction, a longer effective refractory period, and unidirectional conduction block with increasing stretch were observed [26], which were related to the inducibility of AF.

For I_{Na_Mfb}, many studies have been conducted to investigate how this current could influence Mfb proliferation, since fibrotic remodeling was closely related to AF. It has been reported that Na_v 1.5 α-subunit was responsible of I_{Na_Mfb} in human atrial Mfbs, which represented electrophysiological characteristics similar to Na^+ channels found in cardiac excitable cells [11, 44]. Based on this, a multiple parameter exponential function was used in this study, which was modeled after the equation of time courses by Courtemanche et al. to fit the time courses of current decay elicited at depolarized voltages [31]. Unlike the assumption from Koivumäki et al. that V_{rest} of Mfbs resulted in significant inactivation of I_{Na_Mfb}

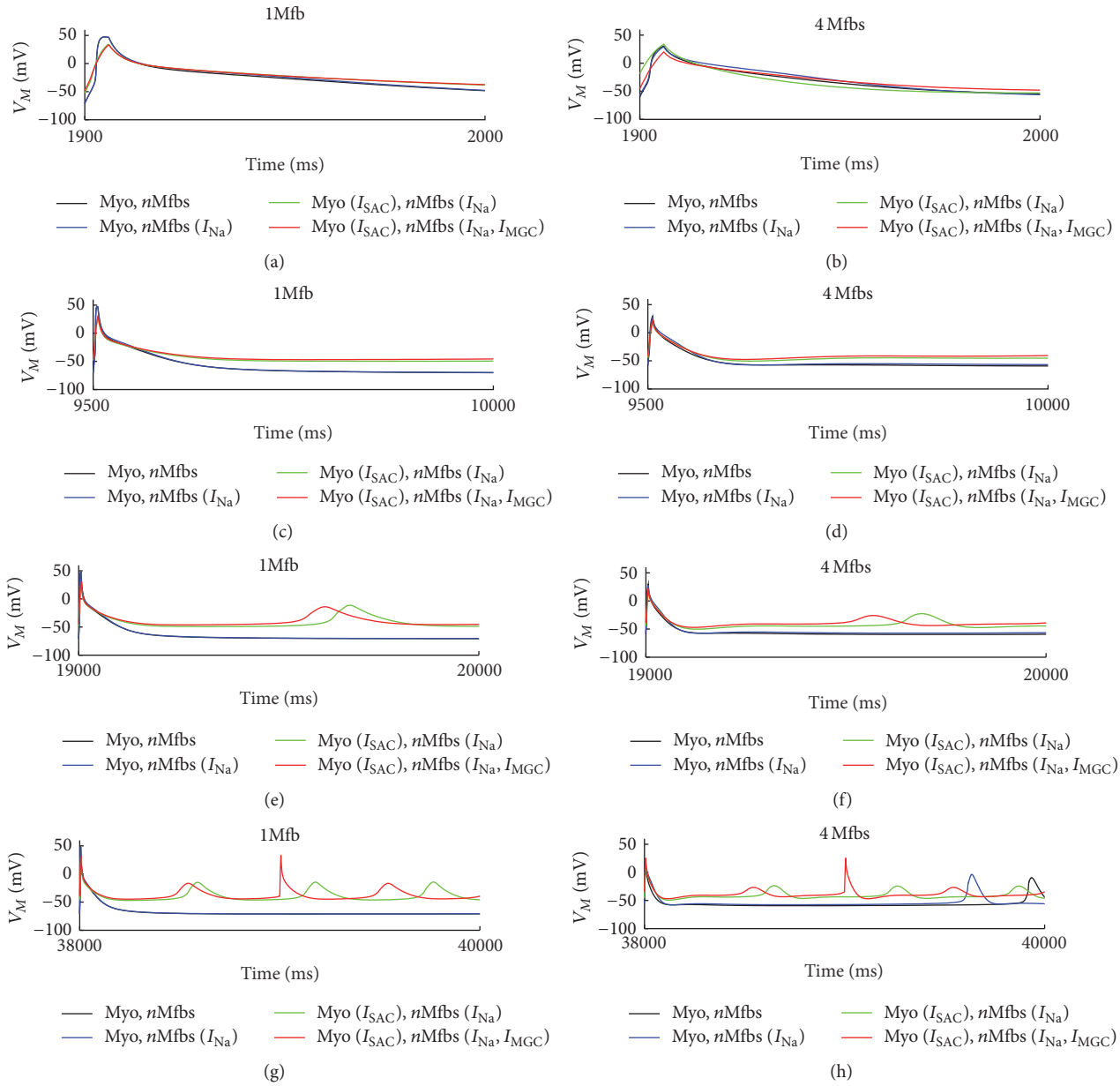

FIGURE 7: Effects of I_{SAC}, I_{Na_Mfb}, and I_{MGC_Mfb} on V_M for several BCLs. (a, b) BCL = 100 ms, (c, d) BCL = 500 ms, (e, f) BCL = 1000 ms, and (g, h) BCL = 2000 ms, in Mfb-M coupling with I_{Na_Mfb} (blue line), with I_{SAC} and I_{Na_Mfb} (green line), and with I_{SAC}, I_{Na_Mfb}, and I_{MGC} (red line) as compared to control (black line), by coupling one and four Mfbs to an atrial myocyte with G_{gap} of 3 nS. Results corresponded to the last cycle in each simulation.

[45], the current was activated during an atrial Mfb AP in our simulations. Our results showed that I_{Na_Mfb} decreased V_{max} and APD_{90} and increased V_{rest} depolarization in myocytes (Figures 4 to 7). Like I_{SAC}, this depolarization would be expected to change diastolic Ca^{2+} levels and conduction velocity.

For I_{MGC_Mfb}, experimental data has indicated that cardiac fibroblasts expressed functional MCGs, contributing to the cardiac mechanoelectrical feedback under both physiological and pathophysiological conditions [18, 19]. Since I_{MGC_Mfb} has been found in Mfbs, we assumed that it could affect Mfb electrophysiological characteristics like I_{SAC} on myocyte. In our simulations, the I-V relation for single MGCs was linear, which agreed with the experimental results [13]. The results showed that integrating I_{MGC_Mfb} in the Mfb model changed the membrane potential of Mfb and further influenced the membrane potential of myocyte by Mfb-myocyte coupling (Figures 4 to 7). Interestingly, MGCs were activated by Mfb compression and inactivated by Mfb stretch [13], implying that I_{MGC_Mfb} should be integrated in

Table 1: Percentage changes in myocyte V_{rest}, V_{max} and APD_{90} as compared to control.

		G_{gap} (nS)		Coupled Mfbs	
		0.5	8	1	4
$V_{max}\downarrow$ (%)	I_{Na_Mfb}	0.8	0.2	0.1	7.9
	I_{Na_Mfb}, I_{SAC}	16.7	23.5	38.1	30.3
	I_{Na_Mfb}, I_{SAC}, I_{MGC_Mfb}	18.6	18.6	37.4	25.9
APD↓ (%)	I_{Na_Mfb}	20.0	1.6	1.1	1.6
	I_{Na_Mfb}, I_{SAC}	19.1	4.1	7.7	8.9
	I_{Na_Mfb}, I_{SAC}, I_{MGC_Mfb}	20.2	11.1	7.8	18.9
$V_{rest}\uparrow$ (%)	I_{Na_Mfb}	8.3	0.8	0.4	2.3
	I_{Na_Mfb}, I_{SAC}	20.3	12.5	25.0	17.4
	I_{Na_Mfb}, I_{SAC}, I_{MGC_Mfb}	22.4	15.9	28.6	23.6

cell modeling only during cell compression, such as fibroblasts/Mfbs compression caused by stretching and dilatation of surrounding cardiac myocytes.

Table 1 shows changes in myocyte V_{rest}, V_{max}, and APD_{90} in three situations as compared to control. The situations were Mfb-M coupling with (1) I_{Na_Mfb}, (2) I_{Na_Mfb} and I_{SAC}, and (3) I_{Na_Mfb}, I_{SAC}, and I_{MGC_Mfb}, respectively. Values were recorded with two Mfbs coupled to a single atrial myocyte in which G_{gap} was varied between 0.5 and 8 nS, or with one and four identical Mfbs coupled to a single atrial myocyte at a constant G_{gap} of 3 nS. In general, it can be seen that I_{Na_Mfb}, I_{SAC}, and I_{MGC_Mfb} played a greater role in reducing V_{max} and APD_{90} and increasing the depolarization of V_{rest} when G_{gap} was relatively small. Increasing the number of coupled Mfbs contributed to a further decline in APD_{90} in all cases, while having different influences on V_{max} and V_{rest}. The reduction of V_{max} and the rise of depolarization of V_{rest} were increased in case (1) and both declined in case (2) and (3).

Previous modeling work suggested that Mfb-M coupling contributed to arrhythmia formation [23, 46]. The key factors included G_{gap}, the number of coupled Mfbs, and Mfb density. Here, we investigated the functional effect of fibrotic remodeling on AF by integrating I_{Na_Mfb}, I_{SAC}, and I_{MGC_Mfb} into Mfb-M coupling. To the best of our knowledge, this has not been examined before. As summarized in Figure 7, these currents made the Mfb act as a current source for the cardiac myocyte, leading to depolarization of V_{rest} and shortening of APD, thereby preserving myocyte excitability to trigger spontaneous excitement and facilitating reentry (such as those of AF).

4.3. Limitations. Two limitations of this mathematical modeling should be mentioned. First, the influence of homologous coupling between adjacent Mfbs was not considered. Since Mfbs can form conduction bridges between myocyte bundles and introduce nonlinearity into Mfb-M coupling to alter electrophysiological properties of the coupled myocyte, coupling between Mfbs may be important in tissue modeling [28, 29]. Second, our modeling of I_{MGC_Mfb} was done using a simplified model based on a linear equation. We did not include the mechanosensitivity of MGCs in our simulation; for example, the conductance depends of the mechanical forces to which the cells are submitted.

5. Conclusions

This study demonstrated the combinational effects of I_{Na_Mfb} and I_{MGC_Mfb} in Mfbs on myocyte excitability and repolarization. Our results showed that the addition of I_{Na_Mfb} and I_{MGC_Mfb} reduced V_{max}, shortened APD, depolarized V_{rest}, and was easy to trigger spontaneous excitement in myocytes. The effects proved that Na^+ current and mechanogated channels in Mfbs should be considered in future pathological cardiac mathematical modeling, such as atrial fibrillation and cardiac fibrosis.

Competing Interests

The authors declare that they have no competing interests.

Acknowledgments

This project is supported by the National Natural Science Foundation of China (81501557).

References

[1] K. S. McDowell, F. Vadakkumpadan, R. Blake et al., "Mechanistic inquiry into the role of tissue remodeling in fibrotic lesions in human atrial fibrillation," *Biophysical Journal*, vol. 104, no. 12, pp. 2764–2773, 2013.

[2] L. Yue, J. Xie, and S. Nattel, "Molecular determinants of cardiac fibroblast electrical function and therapeutic implications for atrial fibrillation," *Cardiovascular Research*, vol. 89, no. 4, pp. 744–753, 2011.

[3] C. Mahnkopf, T. J. Badger, N. S. Burgon et al., "Evaluation of the left atrial substrate in patients with lone atrial fibrillation using delayed-enhanced MRI: implications for disease progression and response to catheter ablation," *Heart Rhythm*, vol. 7, no. 10, pp. 1475–1481, 2010.

[4] B. Burstein, P. Comtois, G. Michael et al., "Changes in connexin expression and the atrial fibrillation substrate in congestive heart failure," *Circulation Research*, vol. 105, no. 12, pp. 1213–1222, 2009.

[5] B. Burstein and S. Nattel, "Atrial Fibrosis: mechanisms and clinical relevance in atrial fibrillation," *Journal of the American College of Cardiology*, vol. 51, no. 8, pp. 802–809, 2008.

[6] C. Vasquez, N. Benamer, and G. E. Morley, "The cardiac fibroblast: functional and electrophysiological considerations in

healthy and diseased hearts," *Journal of Cardiovascular Pharmacology*, vol. 57, no. 4, pp. 380–388, 2011.

[7] N. A. Trayanova, "Mathematical approaches to understanding and imaging atrial fibrillation: significance for mechanisms and management," *Circulation Research*, vol. 114, no. 9, pp. 1516–1531, 2014.

[8] Y. Shibukawa, E. L. Chilton, K. A. MacCannell, R. B. Clark, and W. R. Giles, "K+ currents activated by depolarization in cardiac fibroblasts," *Biophysical Journal*, vol. 88, no. 6, pp. 3924–3935, 2005.

[9] L. Chilton, S. Ohya, D. Freed et al., "K+ currents regulate the resting membrane potential, proliferation, and contractile responses in ventricular fibroblasts and myofibroblasts," *American Journal of Physiology—Heart and Circulatory Physiology*, vol. 288, no. 6, pp. H2931–H2939, 2005.

[10] J. Du, J. Xie, Z. Zhang et al., "TRPM7-mediated Ca^{2+} signals confer fibrogenesis in human atrial fibrillation," *Circulation Research*, vol. 106, no. 5, pp. 992–1003, 2010.

[11] A. Chatelier, A. Mercier, B. Tremblier et al., "A distinct de novo expression of Nav1.5 sodium channels in human atrial fibroblasts differentiated into myofibroblasts," *Journal of Physiology*, vol. 590, no. 17, pp. 4307–4319, 2012.

[12] G.-R. Li, H.-Y. Sun, J.-B. Chen, Y. Zhou, H.-F. Tse, and C.-P. Lau, "Characterization of multiple ion channels in cultured human cardiac fibroblasts," *PLoS ONE*, vol. 4, no. 10, Article ID e7307, 2009.

[13] A. Kamkin, S. Kirischuk, and I. Kiseleva, "Single mechanogated channels activated by mechanical deformation of acutely isolated cardiac fibroblasts from rats," *Acta Physiologica*, vol. 199, no. 3, pp. 277–292, 2010.

[14] A. El Chemaly, R. Guinamard, M. Demion et al., "A voltage-activated proton current in human cardiac fibroblasts," *Biochemical and Biophysical Research Communications*, vol. 340, no. 2, pp. 512–516, 2006.

[15] A. Biernacka and N. G. Frangogiannis, "Aging and cardiac fibrosis," *Aging and Disease*, vol. 2, no. 2, pp. 158–173, 2011.

[16] J. Baum and H. S. Duffy, "Fibroblasts and myofibroblasts: what are we talking about?" *Journal of Cardiovascular Pharmacology*, vol. 57, no. 4, pp. 376–379, 2011.

[17] N. Benamer, H. Moha Ou Maati, S. Demolombe et al., "Molecular and functional characterization of a new potassium conductance in mouse ventricular fibroblasts," *Journal of Molecular and Cellular Cardiology*, vol. 46, no. 4, pp. 508–517, 2009.

[18] A. Kamkin, I. Kiseleva, G. Isenberg et al., "Cardiac fibroblasts and the mechano-electric feedback mechanism in healthy and diseased hearts," *Progress in Biophysics and Molecular Biology*, vol. 82, no. 1–3, pp. 111–120, 2003.

[19] A. Kamkin, I. Kiseleva, I. Lozinsky, and H. Scholz, "Electrical interaction of mechanosensitive fibroblasts and myocytes in the heart," *Basic Research in Cardiology*, vol. 100, no. 4, pp. 337–345, 2005.

[20] M. W. Krueger, K. S. Rhode, M. D. O'Neill et al., "Patient-specific modeling of atrial fibrosis increases the accuracy of sinus rhythm simulations and may explain maintenance of atrial fibrillation," *Journal of Electrocardiology*, vol. 47, no. 3, pp. 324–328, 2014.

[21] P. Comtois and S. Nattel, "Interactions between cardiac fibrosis spatial pattern and ionic remodeling on electrical wave propagation," in *Proceedings of the 33rd Annual International Conference of the IEEE Engineering in Medicine and Biology Society (EMBS '11)*, pp. 4669–4672, IEEE, Boston, Mass, USA, September 2011.

[22] K. Tanaka, S. Zlochiver, K. L. Vikstrom et al., "Spatial distribution of fibrosis governs fibrillation wave dynamics in the posterior left atrium during heart failure," *Circulation Research*, vol. 101, no. 8, pp. 839–847, 2007.

[23] T. Ashihara, R. Haraguchi, K. Nakazawa et al., "The role of fibroblasts in complex fractionated electrograms during persistent/permanent atrial fibrillation: implications for electrogram-based catheter ablation," *Circulation Research*, vol. 110, no. 2, pp. 275–284, 2012.

[24] K. A. MacCannell, H. Bazzazi, L. Chilton, Y. Shibukawa, R. B. Clark, and W. R. Giles, "A mathematical model of electrotonic interactions between ventricular myocytes and fibroblasts," *Biophysical Journal*, vol. 92, no. 11, pp. 4121–4132, 2007.

[25] K. S. McDowell, F. Vadakkumpadan, R. Blake et al., "Methodology for patient-specific modeling of atrial fibrosis as a substrate for atrial fibrillation," *Journal of Electrocardiology*, vol. 45, no. 6, pp. 640–645, 2012.

[26] N. H. L. Kuijpers, H. M. M. Ten Eikelder, P. H. M. Bovendeerd, S. Verheule, T. Arts, and P. A. J. Hilbers, "Mechanoelectric feedback leads to conduction slowing and block in acutely dilated atria: A Modeling Study of Cardiac Electromechanics," *American Journal of Physiology—Heart and Circulatory Physiology*, vol. 292, no. 6, pp. H2832–H2853, 2007.

[27] H. Q. Zhan and L. Xia, "Excitation-contraction coupling between human atrial myocytes with fibroblasts and stretch activated channel current: a simulation study," *Computational and Mathematical Methods in Medicine*, vol. 2013, Article ID 238676, 9 pages, 2013.

[28] M. M. Maleckar, J. L. Greenstein, W. R. Giles, and N. A. Trayanova, "K+ current changes account for the rate dependence of the action potential in the human atrial myocyte," *American Journal of Physiology-Heart and Circulatory Physiology*, vol. 297, no. 4, pp. H1398–H1410, 2009.

[29] M. Miragoli, G. Gaudesius, and S. Rohr, "Electrotonic modulation of cardiac impulse conduction by myofibroblasts," *Circulation Research*, vol. 98, no. 6, pp. 801–810, 2006.

[30] D. Kim, "Novel cation-selective mechanosensitive ion channel in the atrial cell membrane," *Circulation Research*, vol. 72, no. 1, pp. 225–231, 1993.

[31] M. Courtemanche, R. J. Ramirez, and S. Nattel, "Ionic mechanisms underlying human atrial action potential properties: insights from a mathematical model," *American Journal of Physiology—Heart and Circulatory Physiology*, vol. 275, no. 1, pp. H301–H321, 1998.

[32] C.-H. Luo and Y. Rudy, "A dynamic model of the cardiac ventricular action potential. I. Simulations of ionic currents and concentration changes," *Circulation Research*, vol. 74, no. 6, pp. 1071–1096, 1994.

[33] I. Kiseleva, A. Kamkin, A. Pylaev et al., "Electrophysiological properties of mechanosensitive atrial fibroblasts from chronic infarcted rat heart," *Journal of Molecular and Cellular Cardiology*, vol. 30, no. 6, pp. 1083–1093, 1998.

[34] A. Kamkin, I. Kiseleva, K. D. Wagner et al., "Mechanically induced potentials in fibroblasts from human right atrium," *Experimental Physiology*, vol. 84, no. 2, pp. 347–356, 1999.

[35] A. Kamkin, I. Kiseleva, and G. Isenberg, "Activation and inactivation of a non-selective cation conductance by local mechanical deformation of acutely isolated cardiac fibroblasts," *Cardiovascular Research*, vol. 57, no. 3, pp. 793–803, 2003.

[36] A. Kamkin, I. Kiseleva, K.-D. Wagner et al., "A possible role for atrial fibroblasts in postinfarction bradycardia," *American*

Journal of Physiology—Heart and Circulatory Physiology, vol. 282, no. 3, pp. H842–H849, 2002.

[37] A. Kamkin, I. Kiseleva, K.-D. Wagner, I. Lozinsky, J. Günther, and H. Scholz, "Mechanically induced potentials in atrial fibroblasts from rat hearts are sensitive to hypoxia/reoxygenation," *Pflugers Archiv European Journal of Physiology*, vol. 446, no. 2, pp. 169–174, 2003.

[38] L. Chilton, W. R. Giles, and G. L. Smith, "Evidence of intercellular coupling between co-cultured adult rabbit ventricular myocytes and myofibroblasts," *The Journal of Physiology*, vol. 583, no. 1, pp. 225–236, 2007.

[39] M. B. Rook, A. C. G. Van Ginneken, B. De Jonge, A. El Aoumari, D. Gros, and H. J. Jongsma, "Differences in gap junction channels between cardiac myocytes, fibroblasts, and heterologous pairs," *American Journal of Physiology-Cell Physiology*, vol. 263, no. 5, pp. C959–C977, 1992.

[40] M. Zabel, B. S. Koller, F. Sachs, and M. R. Franz, "Stretch-induced voltage changes in the isolated beating heart: importance of the timing of stretch and implications for stretch-activated ion channels," *Cardiovascular Research*, vol. 32, no. 1, pp. 120–130, 1996.

[41] F. Ravelli, M. Disertori, F. Cozzi, R. Antolini, and M. A. Allessie, "Ventricular beats induce variations in cycle length of rapid (type II) atrial flutter in humans. Evidence of leading circle reentry," *Circulation*, vol. 89, no. 5, pp. 2107–2116, 1994.

[42] J.-L. Huang, C.-T. Tai, J.-T. Chen et al., "Effect of atrial dilatation on electrophysiologic properties and inducibility of atrial fibrillation," *Basic Research in Cardiology*, vol. 98, no. 1, pp. 16–24, 2003.

[43] F. Bode, A. Katchman, R. L. Woosley, and M. R. Franz, "Gadolinium decreases stretch-induced vulnerability to atrial fibrillation," *Circulation*, vol. 101, no. 18, pp. 2200–2205, 2000.

[44] W. A. Catterall, A. L. Goldin, and S. G. Waxman, "International union of pharmacology. XLVII. Nomenclature and structure-function relationships of voltage-gated sodium channels," *Pharmacological Reviews*, vol. 57, no. 4, pp. 397–409, 2005.

[45] J. T. Koivumäki, R. B. Clark, D. Belke et al., "Na^+ current expression in human atrial myofibroblasts: identity and functional roles," *Frontiers in Physiology*, vol. 5, article 275, 2014.

[46] S. Zlochiver, V. Muñoz, K. L. Vikstrom, S. M. Taffet, O. Berenfeld, and J. Jalife, "Electrotonic myofibroblast-to-myocyte coupling increases propensity to reentrant arrhythmias in two-dimensional cardiac monolayers," *Biophysical Journal*, vol. 95, no. 9, pp. 4469–4480, 2008.